Photometry and Imaging Results for Comet 9P/Tempel 1 and Deep Impact: Gas Production Rates, Post-Impact Lightcurves, and Ejecta Plume Morphology

David G. Schleicher
Lowell Observatory
1400 W. Mars Hill Road, Flagstaff, Arizona 86001

Kate L. Barnes
Physics & Astronomy Dept., Franklin and Marshall College,
PO Box 3003, Lancaster, PA 17604

Nicole F. Baugh
Lunar & Planetary Laboratory, University of Arizona,
1629 E. University Blvd., Tucson, AZ 85721

Submitted to *The Astronomical Journal*
Original submission: 26 September 2005
Revised and accepted: 28 October 2005
Scheduled for publication: February 2006

The Lowell Observatory Preprint Series

Photometry and Imaging Results for Comet 9P/Tempel 1 and Deep Impact: Gas Production Rates, Post-Impact Lightcurves, and Ejecta Plume Morphology

David G. Schleicher
Lowell Observatory, 1400 W. Mars Hill Rd., Flagstaff, AZ 86001; dgs@lowell.edu

Kate L. Barnes
Physics & Astronomy Dept., Franklin and Marshall College,
PO Box 3003, Lancaster, PA 17604; kate.barnes@fandm.edu

Nicole F. Baugh
Lunar & Planetary Laboratory, University of Arizona,
1629 E. University Blvd., Tucson, AZ 85721; nbaugh@lpl.arizona.edu

ABSTRACT

We present Earth-based imaging and photometry results of Deep Impact target Comet 9P/Tempel 1 obtained at and in the nights surrounding the time of the spacecraft's impact. These observations establish the baseline behavior of Tempel 1 prior to impact, including a water vaporization rate of 6×10^{27} molecules s^{-1}, thereby enabling us to determine the effects directly caused by this explosive event. The instantaneous fireball was not detected, but a post-impact brightening from ejecta material was prominent and shows evidence of a slowly decreasing optical depth over more than an hour of time. We have successfully reproduced both the general morphology of the ejecta plume and many details of the shape and brightness distribution on successive nights following the impact using a modified Monte Carlo jet model, with an initial impulse event in the shape of an open, thick-walled cone. As seen from Earth, the center of the plume is derived to be at a position angle of about 255° and about 20° this side of the plane of the sky, i.e. near the limb of the nucleus. Most of the observed ejecta material had an initial outflow velocity of less than 0.23 km s^{-1}, and particle sizes less than 2.5 microns (assuming compact grains). This resulted in the rapid development of a dust tail from ejecta particles as they are pushed away from the Sun by radiation pressure. Each daughter gas species exhibited an increase in production, with peaks occurring 1-2 days after impact, followed by a gradual decay back to baseline values; the shapes of these lightcurves suggests that the post-impact excess is due to the vaporization of ices within the ejecta over the course of a few days. In nearly all respects, Comet Tempel 1 returned to pre-impact conditions only 6 days after the event.

Key words: comets: individual (9P/Tempel 1) — space vehicles

1. INTRODUCTION

In support of the NASA's Deep Impact spacecraft encounter and collision with Comet 9P/Tempel 1 (A'Hearn et al. 2005a; A'Hearn et al. 2005b; and references therein), we planned and carried out a comprehensive observing campaign of the target. First discovered in 1867, Tempel 1 has been in a relatively stable orbit since its last encounter with Jupiter in 1953 (Yeomans et al. 2005). This first-ever experiment of intentionally colliding a probe with a comet

nucleus to determine the physical structure of the body was designed to be observed both by the flyby spacecraft and by Earth-based telescopes, with a primary goal of learning about the target's properties by examining how it reacts to an explosive release of energy (A'Hearn et al. 2005a). A critical component of such an experiment is to have a detailed understanding of the baseline characteristics of the object, so that effects caused by the impact can be distinguished from normal behavior, such as variations due to the rotation of the nucleus or to orbital motion and changing seasons. Observing campaigns involving hundreds of astronomers were conducted to provide support (Meech et al. 2005a; Meech et al. 2005b). Here we report on photometry and imaging of Tempel 1 obtained at Lowell Observatory at and in the days surrounding the Deep Impact event of 2005 July 4, which provide both a baseline and a detailed look at the impact and its aftermath.

2. INSTRUMENTATION AND REDUCTIONS

In addition to on-going monthly observations of Tempel 1 begun in March 2005 and which will be reported on elsewhere, we obtained 12 consecutive nights of photometric measurements beginning on June 29, and 10 consecutive nights of imaging starting on July 1 (Table 1). A conventional, photoelectric photometer equipped with pulse-counting electronics was first used at the 42-inch (1.1-m) Hall telescope, then switched to Lowell's 31-inch (0.8-m) telescope when the SITe 2048×2048 CCD camera was attached to the Hall telescope on July 1. In 2×2 binning mode, the effective pixel scale of the CCD was 1.18 arcsec per pixel which, when combined with the comet's increasing distance from Earth, corresponds to a plate scale of 752-793 km per pixel during the interval and to 765 km per pixel at the time of impact. Molecular emission bands of CN, C_2, and C_3 were isolated with narrowband filters used with both instruments, along with reflected continuum from dust grains at 4450 and 5260 Å. With the photometer, additional emission bands of OH and NH, along with the continuum at 3448 Å, were also measured with the blue-sensitive phototube, and broadband B and V filters were added for higher S/N lightcurve monitoring on the night of impact. The red-sensitive CCD permitted the use of a narrowband continuum filter at 7228 Å and a broadband R (Kron-Cousins) on each night; a broadband V (Johnson) was also used beginning on July 3. All of the narrowband filters are from the HB comet filter set, which were manufactured in 1996 for Comet Hale-Bopp (Farnham et al. 2000). Images were bias-subtracted and flat-fielded using twilight flats. Each night was photometric and narrowband standard calibration stars (Farnham et al. 2000) were observed, permitting the determination of nightly atmospheric extinction coefficients which were applied to all comet measurements after subtraction of background sky. All narrowband data were then reduced to absolute fluxes and, in the case of emission bands, continuum-subtracted using standard techniques (Farnham et al. 2000). Broadband data were also adjusted to compensate for atmospheric extinction, following sky subtraction and normalization for integration time, but have not been reduced further for the current analyses.

3. PROPERTIES OF TEMPEL 1 PRIOR TO IMPACT

For reference, we first show the comet's appearance just prior to impact on July 4 (Figure 1), where it is evident that the dust coma is very asymmetric with an apparent broad fan of material towards the southeast. Because the red continuum narrowband images are nearly identical in appearance with the R band images, we conclude that gas emission is at most a minor component in the R band filter for Temple 1. With a much higher total throughput and a resulting higher signal-to-noise (S/N), we use the R band images to characterize the dust distribution. Our

monthly imaging with a slowly changing viewing geometry reveals that the fan is actually composed of two components - a dust tail pointing away from the Sun and seen in projection, overlapped by a persistent dust jet or fan which shows little or no rotational variation and so has a source likely located near a rotational pole which continuously remains in sunlight during the pre-perihelion time frame. At the time of the Deep Impact encounter (time from perihelion, ΔT = -1.071 day), the Sun has a position angle (PA) of 290° and a phase angle of 41°, and so the dust tail is at a PA of 110° and is located at an angle of 49° behind the plane of the sky, while the near-polar jet is pointed at a PA of about 130-150° and presumably has a phase angle of less than about 50°, i.e. generally towards the Earth.

In contrast, narrowband CN images not only exhibit a different spatial distribution from the dust, but significant variation from night-to-night (Woodney et al. 2005). We tentatively attribute this variation to rotational effects, presumably due to a second source region on the nucleus, which must be located away from the pole and have a smaller proportion of dust, since a corresponding dust jet is not evident. Since a more extensive analysis of imaging obtained throughout the apparition will be required to decouple rotational variations seen in the gas images from changes induced by Deep Impact, narrowband gas images are not presented here.

Absolute fluxes from the filter photometry were converted to column abundances and production rates for each gas species and to the quantity $A(\theta)f\rho$, a proxy for dust production, for the continuum points using standard techniques and parameters (A'Hearn et al. 1995). Nightly mean values for each species are shown in Figure 2, except for the night of July 4 where we have separately computed pre- and post-impact medians. The pre-impact July 4 value of 5.2×10^{27} molecules s^{-1} for OH corresponds to a water production rate of 6×10^{27} molecules s^{-1}, based on our empirical conversion from Haser OH production rates to vectorial equivalent parent production rates, taking into account the branching ratios during photodissociation and the r_H-dependence of the velocity but making no adjustments for the solar activity cycle (cf. A'Hearn et al. 1995; Cochran and Schleicher 1993). The relative production rates of C_2 to CN place Tempel 1 into the "typical" taxonomic class of A'Hearn et al., consistent with their findings based on the 1983 apparition. In the green continuum passband at 5260 Å, $A(\theta)f\rho$ was about 112 cm just prior to impact, with only a small trend towards smaller values with increasing aperture size. Our value for $A(\theta)f\rho$ is 10% higher than that reported by Keller et al. (2005), possibly due to our smaller phase angle (41°) as compared to that of the Rosetta spacecraft (69°).

Overall, as is evident from Figure 2, gas and dust production on the night of impact showed no evidence of unusual behavior, although some of the previous nights show possible evidence of rotational or sporadic variations (Biver et al. (2005) reported periodic variability of HCN in May). Similar to many short-period comets (A'Hearn et al. 1995), however, Tempel 1 has exhibited a strong seasonal variation in its rate of gas and dust release from the nucleus beyond what would be expected simply due to its changing distance from the Sun, with peak production rates reached 7 weeks prior to perihelion during its 1983 apparition (Osip et al. 1992). This is presumably due to the specific location of one or more isolated active regions coupled with the tilt of the nucleus rotation axis with respect to the orbital plane, thereby changing the amount of solar radiation as the body passes by the Sun. This scenario was quantitatively confirmed for another recent spacecraft target, Comet 19P/Borrelly, which exhibited peak production about 3 weeks prior to perihelion, matching the maximum total solar radiation available predicted by the

source region location and the changing sub-solar latitude as a function of time (Schleicher et al. 2003). A detailed investigation of these issues in the case of Tempel 1 will be the focus of a future paper.

Our 2005 photometric measurements confirm that peak production in Tempel 1 occurred about 6 weeks before perihelion, but with the unexpected finding that production rates overall were substantially lower (1.3× to 2.4×, depending on species) than measured during 1983 (Osip et al. 1992; Lisse et al. 2005), possibly caused by the partial exhaustion or covering over of a source region (Schleicher and Barnes 2005; Schleicher 2005). With this early peak (also measured by Lara et al. 2005), one cannot assume that because the heliocentric distance is nearly constant in the days surrounding perihelion (and Deep Impact), that the production rates would be constant. Indeed, based on measured production rates from early May to late July, we can derive an average rate of decrease for the days near impact of 1% per day for each gas species and for the dust — a small but non-negligible amount. Combining this slope with our best estimate of the pre-impact production rates for each species yields the approximate baselines shown in Figure 2.

4. TIME OF IMPACT AND POST-IMPACT RESULTS

4.1 *July 4*

A major goal of our support observations was to obtain an accurate characterization of the near-instantaneous fireball or flash predicted to result from the collision of the Deep Impact projectile with Tempel 1's nucleus, with a total release of energy equivalent to about 5 tons of TNT in less than one second (A'Hearn et al. 2005a). In particular, we hoped to measure the duration of the flash, in addition to its total brightness. Using the photometer in high-speed mode, we acquired measurements every 0.25 seconds, with 0.20 s integration and 0.05 overhead at each time step, for a total of 180 seconds beginning at 5:51:49 UT, or 24 seconds prior to the predicted time of impact (allowing for light travel time at the distance of Tempel 1). To maximize S/N in these very short integrations, we used a standard broadband V filter. Unfortunately, despite the faintness of the comet's coma, we do not detect any feature in the lightcurve (Figure 3) which can be attributed to the flash at or near the current determination of the time of impact of 5:52:02 UT (A'Hearn et al. 2005b). To coincide with the high time resolution photometry measurements, we also took a 120 second V band image with the CCD starting at 5:51:15 UT. No evidence of the flash from the fireball was detected in the image, either, consistent with numerous other non-detections from a variety of instrumentation (Meech et al. 2005b). Since the Deep Impact flyby spacecraft did detect the fireball and the impact location should have been visible from Earth (A'Hearn et al. 2005b), the lack of Earth-based detections is apparently simply due to insufficient contrast of the fireball to the innermost coma of the comet.

Immediately following the predicted time of impact, a series of broadband R and V images and B and V photometry were obtained to monitor the brightening caused by solar radiation reflected from the newly emitted material in the ejecta plume, interspersed with selected narrowband measurements. As expected, no significant brightening was detected in any of the gas emission band filters on July 4 except for that caused by the brightening of the underlying continuum, because each of the measured gas species is a daughter product of more complex molecules, and the typical lifetimes of the parent species are many hours. In contrast, spectroscopic measurements of parent species in the IR did show rapid brightening following impact (Mumma et al. 2005). Instead, in the 70 minute observing window following impact, we obtained a

lightcurve of the brightening in the reflected continuum (Figure 3). Given the outflow velocity of the ejecta measured on subsequent nights (discussed later), we would expect all of the ejecta to still be within about 2 arcsec of the nucleus at the end of our window on July 4. A simple comparison of the brightness of the central pixel of the comet as a function of time yields an eventual increase in both the V and the R bands of a factor of 6 after 70 minutes. However, the airmass through which we observed Tempel 1 was already ~2.8 at the time of impact and increased to nearly 6.0 when observations were completed, resulting in relatively poor atmospheric "seeing" which got progressively worse with time, spreading the light into more and more pixels. Therefore, the 6× increase is only a lower limit to the actual amount of brightening, and some observers reported an increase of 2.3 magnitudes (Meech et al. 2005b).

A more useful measure of the brightening is obtained by extracting the flux within a series of apertures, and empirically determining how large an aperture is needed, given the degrading seeing, to detect all of the light associated with the ejecta plume. The extracted measurements from this aperture, 13 arcsec in radius, are presented in the middle panel of Figure 3, and this total brightness lightcurve directly tracks the changing total cross section of particles released into the coma as seen from Earth. The lightcurve rises steeply during the first half-hour, and appears to be approaching an asymptotic limit after the 1 hr mark. Since the ejecta would have left the immediate vicinity of the impact site within seconds to minutes of the event, the long interval over which the brightness increases must be due either to an actual increase in surface area caused by fragmenting grains or due to a change in the optical depth of the material. The former could simply occur for a dirty ice conglomerate, where the ice - now exposed to sunlight - vaporizes and releases embedded dust grains. The slow return of gas production rates to baseline levels discussed later implies some ice within the ejecta continues to vaporize for several days, suggesting that at least some fragmentation takes place. However, we believe that the shape of the lightcurve in the first hour following the impact is primarily due to the changing optical depth of the plume. It is clear from imaging by the flyby spacecraft that the ejecta was optically thick during the first quarter-hour, since the newly formed crater is blocked from view by the ejecta (A'Hearn et al. 2005b). As the material moves progressively outward, the particle densities must drop as r^{-2}, eventually becoming optically thin. Assuming that the peak brightness occurred shortly after our last data points and had a value no more than 10% higher than these points, (and consistent with other reports, cf. Meech et al. 2005b), we can estimate that the bulk optical depth would have had a value of unity about 10-12 minutes after impact and a value of ~0.4 about 25 minutes after impact. Unfortunately, different portions of an ejecta cone such as that produced by Deep Impact will become optically thin at different times due to particles having a range of outflow velocities coupled with our view from a somewhat oblique viewing geometry. In fact, we have found no simple expression which reproduces the overall lightcurve: In the first quarter-hour the lightcurve is slightly concave upward, and the material is considerably redder in color than the general inner coma. By about 20-25 minutes after impact, the rate of increase in total cross section becomes negative, beginning the transition to an apparent asymptotic approach to a peak perhaps 1-2 hours after impact. A similar time for this change of slope in the lightcurve was detected by many other observers (cf. Meech et al. 2005; Keller et al. 2005). This transition point is also when the color of the ejecta plume begins to become less red, ultimately reaching a small amount of reddening very similar to that displayed by pre-impact particles in the coma. While this behavior clearly implies a large change in the effective particle size distribution during this

interval, quantitative results must await detailed modeling of the optical depth as a function of time and location within the ejecta plume.

4.2 *July 5-10 — Ejecta Plume Morphology*

By the following night, the ejecta plume had expanded sufficiently to be visible in the imaging but with relatively low contrast to the coma. To examine the ejecta morphology in detail, we both ratioed and differenced each nightly median image to a pre-impact median image, effectively removing the underlying coma. While the ratioed images were very revealing, they were less well suited for subsequent quantitative modeling of the ejecta plume, and so we only show the differenced images in Figure 4. We further enhanced the images by removing a $1/\rho$ radial distribution, to compensate for the decrease in particle column density as material moves outward from the nucleus, and to better determine the distribution of particles within the plume as a function of time (also shown in Figure 4). While it might first appear that the center of the plume is towards the southwest, with a breadth of more than 180°, a detailed examination of the day by day evolution reveals two distinct components. One part is an arc-like structure moving radially outward centered at a nearly westerly direction, while the second part is a more diffuse feature arising from the plume material after it is pushed away from the Sun by radiation pressure, i.e. a dust tail created by the plume material itself. On July 5th, only the lightest particles have been blown back, but by the 7th more material is in the plume tail than remains in the original plume. At the end of the sequence, the overall inner coma has dropped back and even below pre-impact values, with the only plume remnants now in the tailward direction, except at the innermost pixels surrounding the nucleus where an enhancement continues to persist. Given the spatial scales and the duration, this near-nucleus enhancement must be due to large, heavy particles which have outflow velocities averaged over a 6-day interval of <1 m s^{-1} and might therefore be gravitational bound to the nucleus; based on the derived mass and gravity of the nucleus as determined by A'Hearn et al. (2005), the escape velocity at the surface of the nucleus is about 1.7 m s^{-1}. In comparison, the leading edge of the plume on July 5th (23 hrs after impact) was at a projected distance of 18,000 km, for an average projected velocity of 0.22 km s^{-1}, consistent with other determinations (cf. Meech et al. 2005b). This velocity rapidly decreased, for an average value between July 6th and 5th of 0.08 km s^{-1} and to 0.03 km s^{-1} between the 7th and the 6th, due to the effects of solar radiation pressure.

To test this scenario for the plume evolution, we modified an existing Monte Carlo dust jet model originally developed to model observed spiral dust jets in Comets Hale-Bopp (Farnham et al. 1999; Farnham and Schleicher 2002) and Hyakutake (Schleicher and Woodney 2003) using an empirical approach: In our model, the orientation of the nucleus, the size and location of source regions, the width and outflow velocity of the jets, and the particle sizes are all adjustable parameters, and we systematically search this multi-dimensional parameter space to reproduce the observed jet morphology as a function of time and changing viewing geometries. Major modifications made to the model for an impact scenario included 1) an impulse release of particles rather than on-going outgassing driven by available solar heating, and 2) an outflow spatial distribution with an open cone having an adjustable breadth and adjustable wall thickness rather than a jet with a Gaussian cross-section. The need for this second modification quickly became apparent in our initial modeling as no jet with a Gaussian cross-section could reproduce the basic arc-like structure without being much brighter in the center than towards the sides of the jet, whereas the observed feature has a nearly uniform brightness along most of the arc.

Because of the impulse nature of the event, the rotation period of the nucleus and even the orientation of the rotational axis could be ignored; we simply assumed an arbitrary orientation and converted our solution for the location of the impact crater into a position on the nucleus as viewed from Earth. And because the position of the crater as determined by the spacecraft team from Deep Impact imaging was not yet available when we performed our modeling, our solution is completely independent from the spacecraft results (A'Hearn et al. 2005b), thereby providing an additional test of our model.

Free parameters in our model included the crater location, the opening angle of the cone, the FWHM of the cone wall, along with the outflow velocities of the particles, and the effective sizes of the particles and therefore the acceleration away from the Sun due to radiation pressure. Particles are modeled as compact, isotropic scatterers, to minimize the number of free parameters. Ultimately, and somewhat surprisingly, the best solution we determined for each parameter was largely decoupled from the other parameters. This both simplified the search of parameter space, and resulted in a more tightly constrained solution than we anticipated. For instance, any solution having the center of the plume (i.e. the assumed normal direction) at a position angle north of west (>270°) resulted in either a much too short of an arc or to a large amount of material blown back into the northeast quadrant by radiation pressure which we do not observe. Even the thickness of the cone wall was tightly constrained, with a too narrow wall resulting in the ends of the arc much brighter than the center, while a wall too thick begins to resemble our original Gaussian jet and is again too bright at the center of the arc. When performing our parameter search, we "viewed" the model as seen from Earth, comparing the model (with no underlying coma and with a $1/\rho$ distribution removed from the Monte Carlo result) to the images from Figure 4. Specifically, we overlaid the model display with measurements of the distance to the peak brightness and to the leading edge of the plume at 10° steps in position angle, thereby allowing a quantitative match of the shape of the plume. In addition, we also attempted to match the relative intensities as a function of position angle and projected distance from the nucleus.

Our best model solution has the following values for key parameters, along with estimated uncertainties based on when the model fit became noticeably worse: A position angle of the center of the ejecta plume of 255° (±10°) and a "phase angle" (where 0° is towards the Earth, 90° is on the limb of the nucleus) of 70° (±15°), an outflow velocity with a distribution of values between about 0.13 and 0.23 km s^{-1}, a lower limit to the radiation pressure parameter β of about 0.24, particle diameters ranging between 0.5 and 2.5 microns (assuming spherical particles and densities of 1 gm cm^{-3}; porous particles would be correspondingly larger in size), a cone opening angle (wall center to wall center) of 70° (±5°) and a cone wall thickness (FWHM) of 30° (±8°). Combining these last two parameters yields an approximate total cone width of 100° based on the exterior wall half-power points. The resulting model morphology for each night after impact is presented in Figure 4 and as an animation[1], which we consider to be a very good match to the observations, especially given the relatively simple nature of our model assumptions. The only significant departure of the model from the images is due to the lack of coupling in our model of the range of outflow velocities with the range of particle sizes. While in a normal cometary jet the lightest particles can be assumed to have the highest velocities, it was not evident *a priori*

[1]Tempel 1 ejecta plume and model at: http://www.lowell.edu/Research/comets.html

that this should or would be the case for the ejecta from a cratering event. But the deviations of our model from the data can readily be explained if the particles having the fastest outflow velocities indeed are systematically at the small end of the derived size range. This conclusion was also reached by Harker et al. (2005) based on the derived particle size distribution of the ejecta as a function of time from thermal modeling of mid-IR Gemini observations.

As a test of our model and our preferred solution, we subsequently compared our derived impact location to a preliminary shape model of the nucleus as viewed from Earth along with the crater location and associated normal direction (Farnham, personal comm.). In this shape model, the normal direction has a position angle of 242° and a "phase angle" of about 65°, or only 14° from our value of the center of the ejection cone, confirming the basic validity of our model. It is as yet unclear whether this 14° difference is simply associated with our model uncertainties, or an incorrect but necessary assumption in our model such as an azimuthally symmetric cone, or is instead providing an indication that the ejecta cone was not released normal to the surface; the direction of the offset in positions is consistent with that expected if the ejecta cone has a down-range component due to the shallow impact angle of the impactor of 20-40° to the horizontal (A'Hearn et al. 2005b). High-spatial resolution imaging obtained in the first hours after impact should help clarify the situation; for instance, Sugita et al. (2005) claimed a fan-shaped plume was centered at a position angle of 225°, based on thermal-IR images, while HST images exhibit an asymmetric plume (brighter towards the west) centered near a PA of 235° (Feldman et al. 2005). In any case, it is clear that Earth-based imaging of the evolution of the ejecta plume provides strong constraints on the physical nature of the plume, and improved models will result when both spacecraft and Earth-based images are utilized.

4.3 *July 5-10 — Production Rates*

Returning to the narrowband photometry measurements on the nights following the impact, computed gas production rates peaked either on July 5 or 6 before progressively dropping back at approximately the same rate of decay for all species (Fig. 4). We note that, because of the nature of the impact event and ejecta plume, the standard Haser model used in the computation of production rates as well as the $A(\theta)f\rho$ proxy for dust production yield only approximations of the actual ongoing production of gas and dust, potentially yielding artificially high values. The values are most problematic on July 5; by July 6 the derived gas production rates show almost no trend with aperture size, implying that the radial spatial distributions of each gas species assumed by the Haser model adequately match the actual distributions. Unfortunately, the scatter evident among the pre-impact data for some species makes it difficult to always determine precise baseline values (our best estimates are shown in Figure 2), but it appears that all species have returned very close to pre-impact values and even to nominal baseline values by our last night of observations on July 10. Since each species has differing parent and daughter lifetimes, ranging from a few hours to a few days at Tempel 1's distance from the Sun, the similar rates of decrease in the days following July 5 and 6 imply an ongoing but diminishing vaporization of ice either within the ejecta plume or ejecta which has settled back onto the surface of the nucleus. In fact, it is believed that a large fraction of the ejecta material was lifted at such low velocities that it did not attain escape velocity (Richardson et al. 2005; Schultz et al. 2005). While the similar post-impact lightcurves among the gas species, especially in the cases of CN and C_2 whose abundance ratio defines the primary compositional classification scheme of A'Hearn et al. (1995), might imply that the ejecta has the same composition as the overall coma, this result must be

considered suggestive rather than definitive because of the previously mentioned inadequacies of the Haser model in a non-equilibrium situation. In particular, the July 5 production rates are likely to be upper limits on the actual amount of excess material associated with the impact, and the degree to which an extrapolation to the whole coma from aperture measurements will be incorrect will vary with the lifetimes of each species.

In contrast to the gas lightcurves, the derived dust production drops more rapidly and, based on the imaging already discussed, appears to simply track the motion of the dust grains out of the photometer aperture. In fact, there is no evidence of the ongoing release of additional dust resulting from the impact, and the data are consistent with *no* significant increase in outgassing due to a possible new source region at the impact crater. This, however, is not surprising as the crater is presumably much smaller (<1%) than the ~2 km^2 total active area required to produce the baseline water production (A'Hearn et al. 1995; Cowan and A'Hearn 1979), and therefore below our detection threshold. The integrated excess water production following the impact yields an upper limit to the total number of water molecules associated with the ejecta of 4×10^{32}, corresponding to about 13 million kg of ice or the equivalent of a cube about 23 m on a side. In comparison, measurements from the Rosetta spacecraft yield a total water release associated with the impact of about 5 million kg (Küppers et al. 2005), a result which is less dependent on the assumed spatial distribution of the OH than our own value which is necessarily an upper limit as discussed earlier in this section.

5. A SUMMARY SCENARIO

We conclude with a summary scenario for the resulting effects of the Deep Impact collision with Comet Tempel 1: The release of ejecta can be approximated as an impulse event, with a rapid brightening of the inner-most coma, followed by a more gradual brightening for more than an hour, likely caused by portions of the ejecta cone progressively becoming optically thin. While moving outward on successive nights, the velocity of the leading edge of the cone, i.e. the outer edge of the observed arc as seen from Earth, slowed rapidly due to radiation pressure from the Sun, and the lightest particles were quickly pushed back, forming an ejecta "tail." The shape and motion of the ejecta cone and tail provide strong constraints on the sizes and velocities of the grains and the width and thickness of the initial ejecta plume. A relatively simple open cone model with thick walls can successfully reproduce the temporal evolution of the plume morphology, and we derive effective particle sizes ranging between about 0.5 and 2.5 microns and initial velocities of less than 0.23 km s^{-1}. Excess gas production likely continued for a few days, presumably until the volatile content of the ejecta material was exhausted. These results, when combined with the flyby spacecraft observations shortly after impact, should ultimately yield a much better understanding of the physical structure of the surface of Comet Tempel 1.

ACKNOWLEDGEMENTS

We thank L. Woodney for assisting with software used in the image reduction and analyses, T. Farnham for providing viewing geometries used in the Monte Carlo model and assistance in the original model creation, and M. A'Hearn and T. Farnham for providing Deep Impact results prior to publication and many useful discussions. This research has been supported by grants from NASA's Planetary Astronomy Program and by the NSF REU program.

REFERENCES

A'Hearn, M. F., Belton, M. J. S., Delamere, A., & Blume, W. H. 2005a, Space Science Reviews 117, 1.

A'Hearn, M. F., Millis, R. L., Schleicher, D. G., Osip, D. J., & Birch, P. V. 1995, Icarus 118, 223.

A'Hearn, M. F., et al. 2005b, Science, in press.

Biver, N., Bockelee-Morvan, D., Colom, P., Crovisier, J., Lecacheux, A., & Paubert, G. 2005, IAU Circular 8538.

Cochran, A. L., & Schleicher, D. G. 1993, Icarus 105, 235.

Cowan, J. J., & A'Hearn, M. F. 1979, Moon and Planets 21, 155.

Farnham, T. L., & Schleicher, D. G. 2002, in IAU Colloquium No. 186, Cometary Science After Hale-Bopp, Abstract Book, p. 15.

Farnham, T. L., Schleicher, D. G., & A'Hearn, M. F. 2000, Icarus 180, 147.

Farnham, T. L., Schleicher, D. G., Williams, W. R., & Smith, B. R. 1999, B.A.A.S. 31, 1120.

Feldman, P. D., Weaver, H. A., A'Hearn, M. F., Belton, M. J. S., & Meech, K. J. 2005, B.A.A.S. 37, 709.

Harker, D. E., Woodward, C. E., & Wooden, D. H. 2005, Science, in press.

Keller, H. U., et al. 2005, Science, in press.

Küppers, M., et al. 2005, Nature 437, 987.

Lara, L. M., Boehnhardt, H., Gredel, R., Gutiérrez, P. J., Ortiz, J. L., Rodrigo, R., & Vidal-Nuñez, M. J. 2005, A&A, in press.

Lisse, C. M., A'Hearn, M. F., Farnham, T. L., Groussin, O., Meech, K. J., Fink, U., & Schleicher, D. G. 2005, Space Science Reviews 117, 161.

Meech, K. J., A'Hearn, M. F., Fernández, Y. R., Lisse, C. M., Weaver, H. A., Biver, N., & Woodney, L. M. 2005a, Space Science Reviews 117, 297.

Meech, K. J., et al. 2005b, Science, in press.

Mumma, M. J., et al. 2005, Science, in press.

Osip, D. J., Schleicher, D. G., & Millis, R. L. 1992, Icarus 98, 115.

Richardson, J. E., Melosh, H. J., & Deep Impact Science Team 2005, B.A.A.S. 37, 703.

Schleicher, D. G., 2005, B.A.A.S. 37, 713.

Schleicher, D., & Barnes, K. 2005, IAU Circular 8546.

Schleicher, D. G., & Woodney, L. M. 2003, Icarus 162, 190.

Schleicher, D. G., Woodney, L. M., & Millis, R. L. 2003, Icarus 162, 415.

Schultz, P. H., & Deep Impact Science Team 2005, B.A.A.S. 37, 704.

Sugita, S., et al. 2005, Science, in press.

Woodney, L. M., Barnes, K. L., Baugh, N. F., & Schleicher, D. G. 2005, B.A.A.S. 37, 647.

Yeomans, D. K, Giorgini, J. D., & Chesley, S. R. 2005, Space Science Reviews 117, 123.

FIGURE CAPTIONS:

Figure 1. — R band median image (from 4 frames) of Comet Tempel 1's dust coma on 2005 July 4 obtained in the interval of 91 and 3 minutes before the Deep Impact encounter. North is at the top and east is towards the left, while the Sun is towards the upper-right at a PA of 290°. The field is 150,000 km on a side. Both views have been stretched logarithmically, but the right-hand panel has first had a canonical $1/\rho$ radial profile removed (ρ is the projected radial distance as seen in the plane of the sky) to make the bulk dust coma asymmetry towards the southeast more visible. The dark dot at the center of the enhanced image is caused by the $1/\rho$ distribution removing too much light at the center of the comet because of seeing blur in the data. The bulk excess towards the southeast is due to the overlap of a dust tail at a PA of 110° and a persistent polar jet at a PA of 130-150°. The background features visible in the median image are caused by the residual overlapping wings of stars from frame to frame.

Figure 2. — Production rates as a function of time from perihelion (July 5.32). Nightly means are plotted for each species, except on July 4 when separate averages are computed for the pre-impact measurements (filled) and for the post-impact data points (open). The time of impact (ΔT = -1.071 day) is indicated on each panel with an arrow. On most nights, 3-4 data sets were obtained using aperture radii varying between 11,000 and 31,000 km at the distance of the comet, but only a single, high airmass set was acquired on July 2. Only dust exhibits an increase on July 4 immediately following the encounter, presumably because little of the gas has had sufficient time to dissociate into the observable daughter gas species. By July 5, all species except for the low S/N NH exhibit a significant increase over pre-impact values; by July 7 the excess production of each species is noticeably decreasing, with similar rates for all of the gas species (except for the very short-lived C_3), eventually returning to approximate baseline values (dashed lines) by the last day of observation, July 10.

Figure 3. — Lightcurves at and following the Deep Impact encounter. TOP) High time resolution photometric measurements surrounding the time of the expected flash from the impactor's fireball. The relatively large amount of scatter is due to a combination of photon statistics and atmospheric scintillation noise associated with the short (0.2 s) integration times. Overlaid are a median smooth curve and a linear fit to the data. We do *not* detect any evidence of a flash at or near the nominal time of impact (5:52:02 UT; vertical dotted line), but a slight upward trend may be associated with the initial brightening from plume material. MIDDLE) Lightcurve of the post-impact brightening on July 4. Total brightness increases were extracted from each image after first subtracting a pre-impact median image to remove the background coma contribution. We have arbitrarily scaled the V band points (open) to best match the R band data (filled) during the first 20 minutes. Note that both a significant change in curvature and in color begins to occur about 20-25 minutes after impact. BOTTOM) Lightcurves of the total brightness excess in the R band on the nights subsequent to the impact. Filled circles are extracted brightness using the same 13 arcsec radius aperture as in the middle panel (corresponding to a radius of 1.0×10^4 km); most of the plume material has already moved beyond this aperture only one day after impact. Fluxes from a much larger aperture, having a radius of 4.6×10^4 km, are shown with filled triangles. Similar to the gas production rate results shown in Figure 2, the dust has also returned to pre-impact values by July 10.

Figure 4. — Daily sequence of ejecta plume images. A single R band post-impact image obtained 44 minutes after impact is shown on July 4, while nightly medians are used on all subsequent nights. Each R band image is first differenced with a median R image from frames obtained on July 4 before the time of impact, effectively removing the original dust coma and with the results shown in the top row. Each image is 120,000 km on a side. The primary ejecta plume is generally towards the west (right), and is subsequently pushed back towards the southeast (lower-left) by radiation pressure from the Sun. The progressive darkening of the center of the coma near the end of the sequence is due to the seasonal drop in production rates, coupled with ratioing each image to the pre-impact image which has not been adjusted for this trend with time. An inner-most coma enhancement is visible at the end of the sequence, presumably caused by a population of either very slow moving (<1 m s^{-1}) or gravitationally bound grains. Because column densities naturally decrease with distance from the nucleus as material moves outward, following the differencing we have also removed a 1/ ρ profile to better view the motion of the ejecta plume (middle row). In the bottom row, we display a corresponding model of the ejecta plume, from which we also removed a 1/ ρ profile to allow direct comparison to the images displayed in the middle row. Our best solution is of an impulse ejecta cone having a peak opening angle of 70° with a Gaussian wall with a FWHM thickness of 30°. Most material has an initial outflow velocity of between 0.13 and 0.23 km s^{-1}. The normal direction of the plume as seen from Earth has a position angle of about 255° and a phase angle of about 70°, i.e. close to the limb but on the Earth-facing hemisphere. The Sun is at a position angle of 290° and within only a few days has turned around most ejecta particles and formed an plume "tail" which has mostly dispersed by the last day in our sequence. The observations are best reproduced with particles having effective diameters ranging between 0.5 and 2.5 microns.

TABLE 1
Observing Circumstances for Photometric Measurements of Comet Tempel 1.

UT Date	# of Obs	r_H (AU)	Δ (AU)	v_H (km s^{-1})	Phase Angle (°)	Position Angle (°)	Broadband CCD Filters
June 29.22	4	1.507	0.869	–0.7	40.4	290.6	—
June 30.24	4	1.507	0.874	–0.6	40.6	290.5	—
July 1.25	2	1.507	0.879	–0.5	40.7	290.4	R
July 2.27	1	1.506	0.884	–0.4	40.8	290.3	R
July 3.22	4	1.506	0.889	–0.2	40.9	290.2	V, R
July 4.23	4	1.506	0.894	–0.1	40.9	290.1	V, R
July 5.21	4	1.506	0.899	+0.0	41.0	290.0	V, R
July 6.22	4	1.506	0.905	+0.1	41.1	289.9	V, R
July 7.20	3	1.506	0.910	+0.2	41.2	289.8	V, R
July 8.20	3	1.506	0.915	+0.3	41.2	289.7	V, R
July 9.20	3	1.507	0.921	+0.5	41.3	289.6	V, R
July 10.20	3	1.507	0.926	+0.6	41.4	289.5	V, R

Notes — The listed UT dates are mid-times of the photometer observations, r_H and v_H are the heliocentric distance and velocity, respectively, Δ is the geocentric distance, and the phase angle and position angle are for the Sun. Imaging was obtained on the nights July 1-10. Narrowband HB comet filters were used each night (see text) and, in addition to the CCD broadband filters listed, broadband B and V filters were used with the photometer on July 4, the night of impact.

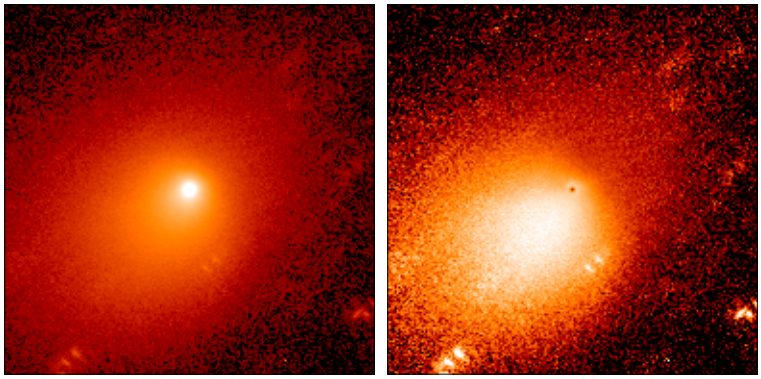

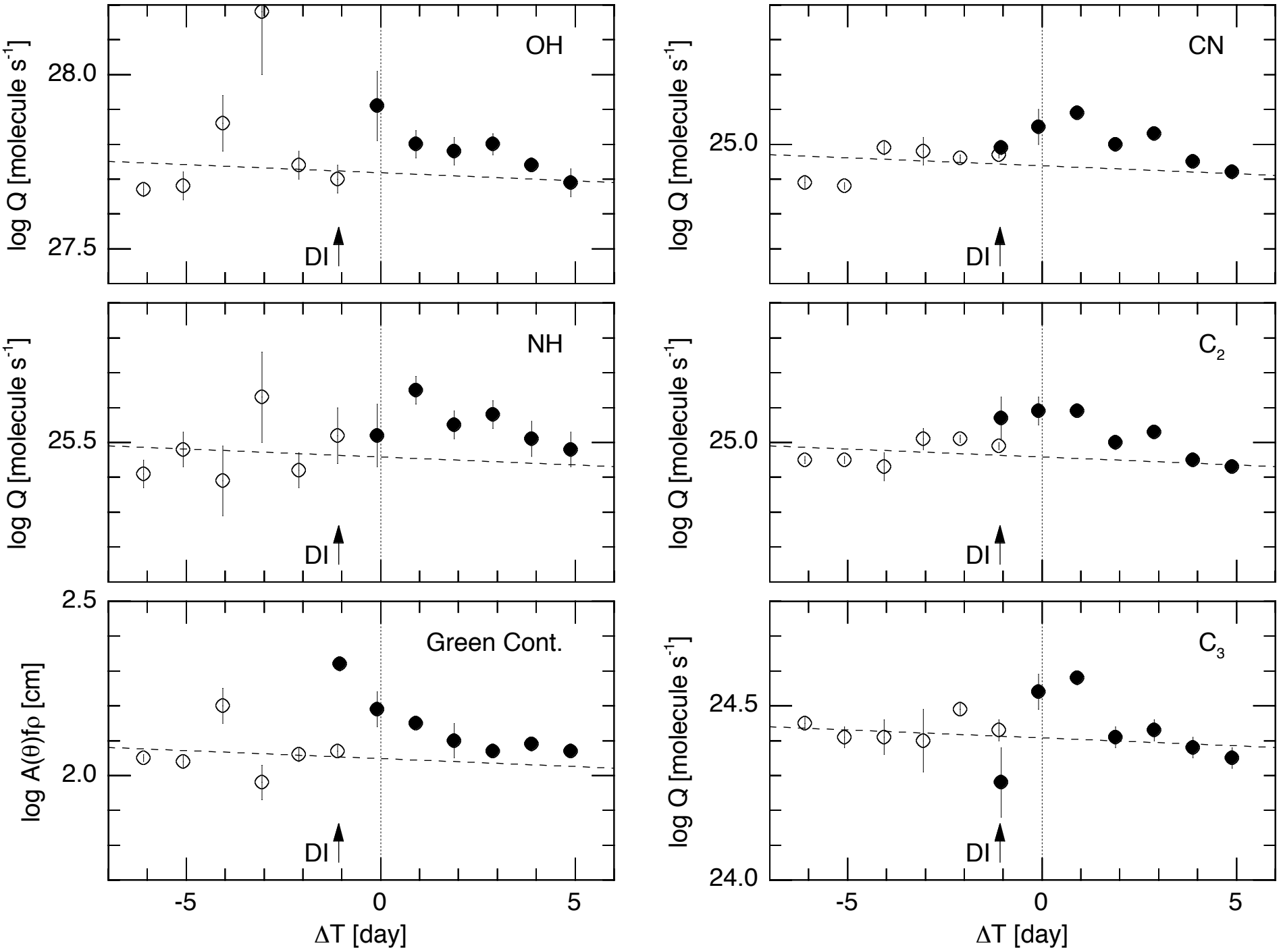
OH
NH
Green Cont.
CN
C2
C3
DI
log Q [molecule s-1]
log A(θ)fρ [cm]
28.0
27.5
25.5
2.5
2.0
25.0
24.5
24.0
-5
0
5
ΔT [day]

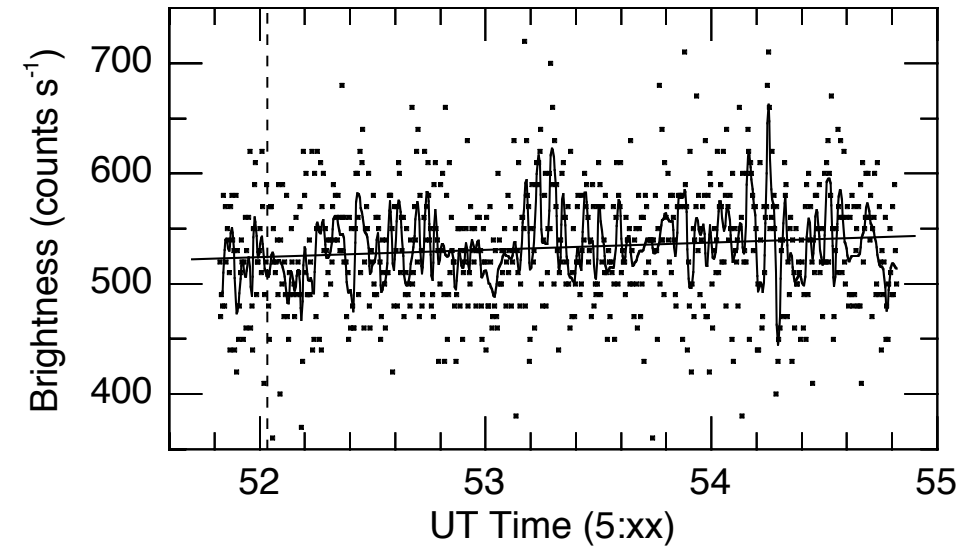
Brightness (counts s-1)
700
600
500
400
52
53
54
55
UT Time (5:xx)

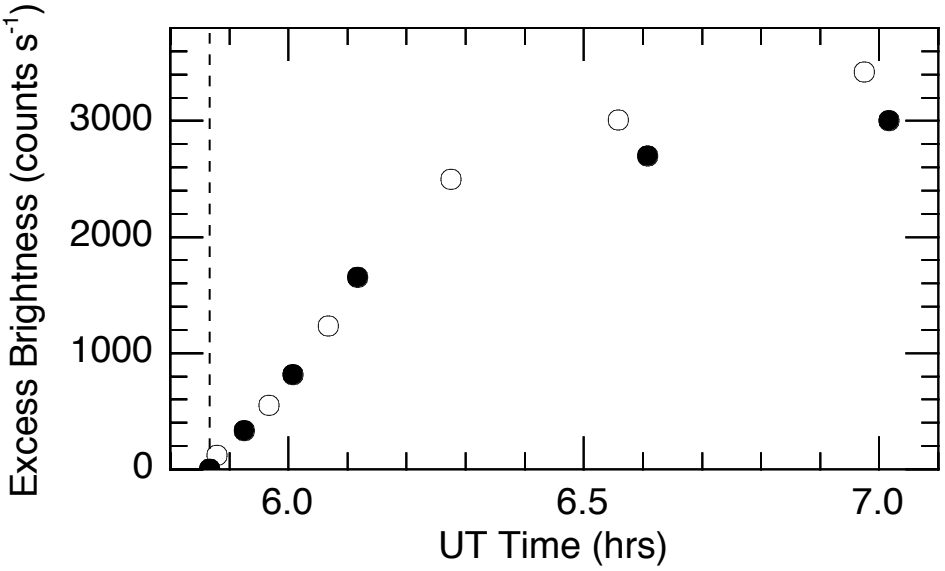
Excess Brightness (counts s-1)
3000
2000
1000
0
6.0
6.5
7.0
UT Time (hrs)

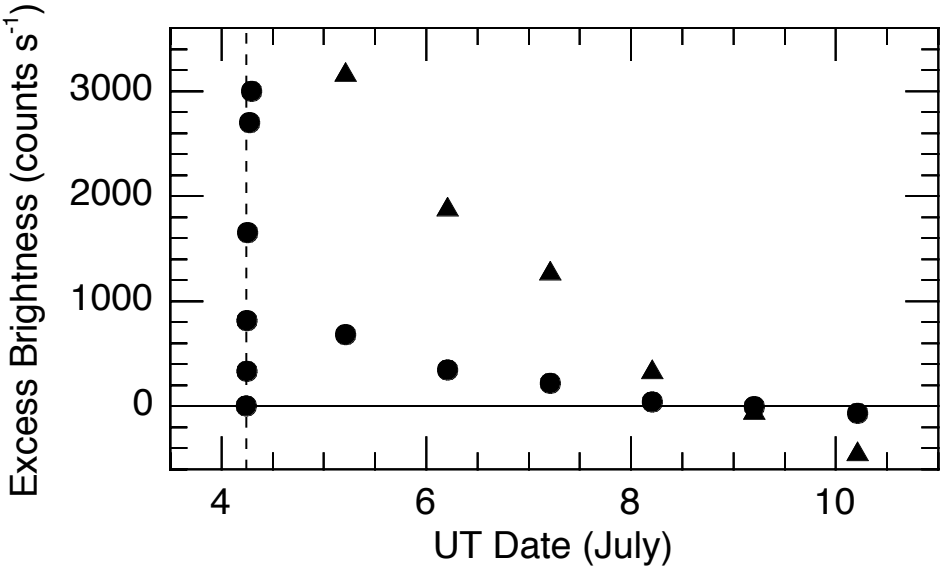
Excess Brightness (counts s-1)
3000
2000
1000
0
4
6
8
10
UT Date (July)

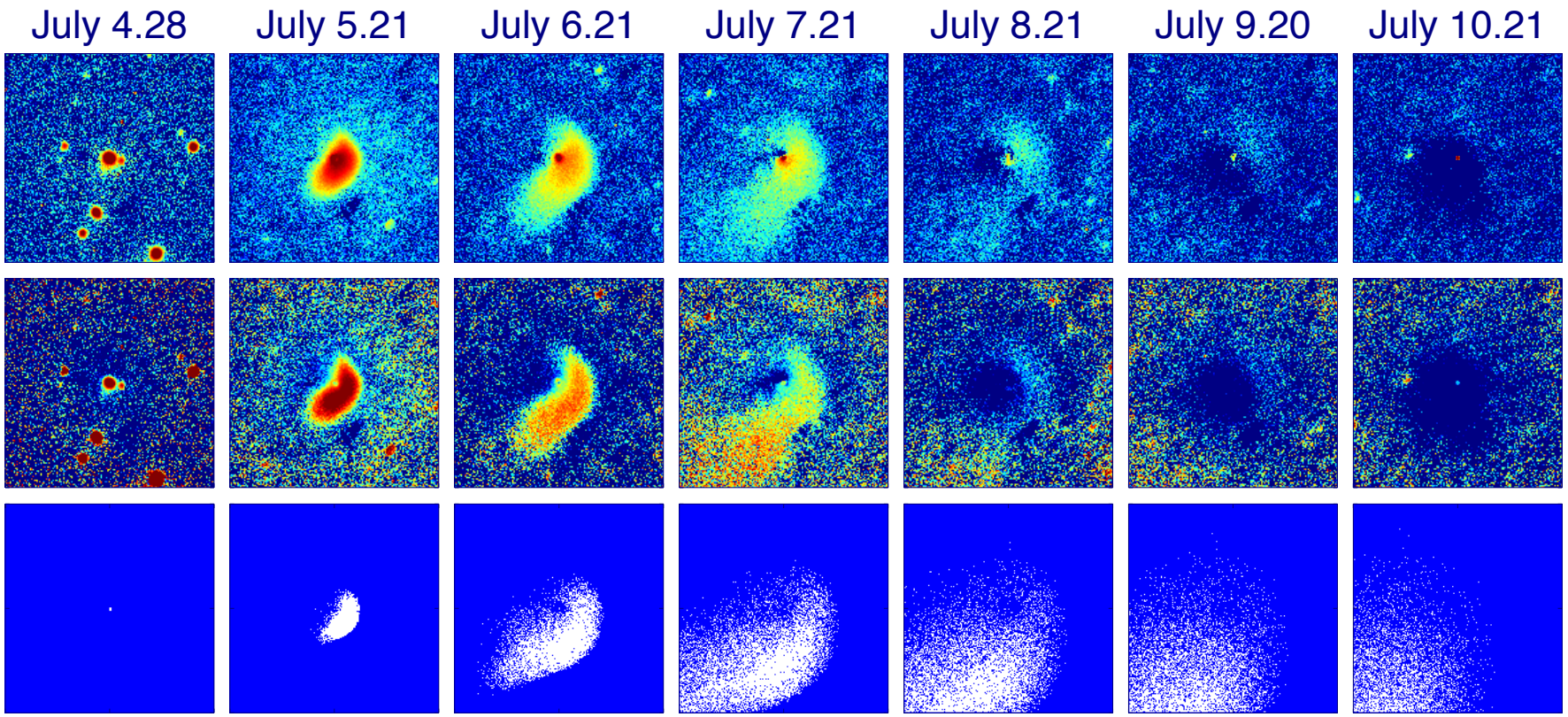
July 4.28
July 5.21
July 6.21
July 7.21
July 8.21
July 9.20
July 10.21